The Dynamics of Superbubbles in the Large Magellanic Cloud

M.S. Oey[1]
Steward Observatory, University of Arizona, Tucson, AZ 85721

ABSTRACT

Based on the stellar populations observed within this sample of LMC superbubbles, I use a numerical version of the standard, pressure-driven bubble model to investigate the shell dynamics. The results fall into two distinct categories corresponding to a subset of objects for which the observed expansion velocity is too large for the observed shell radius ("high-velocity" superbubbles), and a subset of objects which appears more dynamically consistent with the model ("low-velocity superbubbles"). Both subsets of objects imply an overestimate in the shell growth rate equivalent to an overestimate in input power by up to an order of magnitude. The high-velocity objects exhibit X-ray evidence of supernova activity, suggesting that the dynamical discrepancy is due to acceleration by SNR impacts.

Subject headings:

1. Introduction

In recent years, we have come to better appreciate the profound interaction between massive stars and the interstellar medium (ISM). A particular realization that has emerged is the dominance of strong stellar winds and supernovae in the energetics and structuring of the ISM (*e.g.,* Abbott 1982), and the consequences for star formation and galaxy evolution. The resultant superbubbles and giant shells around OB associations and starbursts are therefore the nexus in this cycle between massive stars and their environment. Furthermore, the evolution of these superbubbles is also a critical component in determining the amount and distribution of the hot interstellar component.

For the last two decades, we have used the "standard model" for a pressure-driven wind bubble, described by *e.g.,* Weaver *et al.* (1977) and Castor, McCray, & Weaver (1975) to interpret shell structures. While extensions have been contributed over the years to explore varying physical details (*e.g.,* McKee *et al.* 1984; Mac Low & McCray 1988; Koo & McKee 1992a, b), the standard model remains unmodified. Indeed, there has been little opportunity to test the model's

[1]Present address: Institute of Astronomy, Madingley Road, Cambridge CB3 0HA, United Kingdom; oey@ast.cam.ac.uk.

dynamical predictions due to loose constraints on the input parameters. The input wind power, in particular, has been difficult to constrain without detailed knowledge of the parent stellar population. Although this fact has long been appreciated (*e.g.,* Braunsfurth & Feitzinger 1983; Rosado 1986), detailed censuses of OB associations require individual spectral classifications, and have not become available until more recently (*e.g.,* Massey *et al.* 1989a, b).

However, detailed studies of OB associations in the Magellanic Clouds are now routinely possible with CCD photometry and slit or multi-fiber spectroscopy. Similar studies are also possible in the Galaxy, especially with the advances in infrared imaging and spectroscopy. With specific knowledge of the massive star population within any given superbubble, it is possible to constrain the input wind power and also the age of the system. Two studies of OB associations in the Galaxy, Cygnus OB1 (Saken *et al.* 1992) and Orion OB1 (Brown *et al.* 1995), have been used in conjunction with the standard model, to examine the surrounding superbubbles. Although these studies only used analytic formulations, both found a discrepancy with the model such that the shell radius appeared too small to be consistent with the observed stellar population.

The only other aspect of the model that has been tested is the prediction of soft X-ray emission, with mixed results. Chu & Mac Low (1990) and Wang & Helfand (1991) found a majority of superbubbles with X-ray luminosities an order of magnitude in excess of that predicted by the standard model. Both papers suggested that supernova remnants (SNRs) striking the shell wall could explain this X-ray excess. More recently, Arthur & Henney (1995) have suggested mass-loading from clumps in a post-shock SNR flow as an alternative explanation. On the other hand, Martin & Kennicutt (1995) suggest mass-loading from pre-existing clumps in the ambient medium to explain X-ray excess in a supergiant shell. Does the X-ray luminosity signal an energy loss mechanism, and therefore imply a discrepancy with the adiabatic standard model? Or is the adiabatic model essentially correct, with occasional disturbances due to supernovae (SNe)? Chu *et al.* (1995) report new observations of superbubbles with limits on X-ray luminosities that are consistent with the standard model, demonstrating that not all superbubbles have X-ray excesses.

With the role that the supershell phenomenon plays in galactic structure and evolution, it is vital to establish the relevance of the standard model and understand the dominant dynamical processes. The current study is part of a comprehensive project to examine a sample of superbubbles in detail, both with regard to the stellar content and the nebular properties, with the aim of these objectives. Given the obscuration, distance, and membership uncertainties in Galactic OB studies, I have turned my attention to the clusters of the Large Magellanic Cloud (LMC). This neighboring galaxy presents a wealth of superbubbles with an unobscured view of both the nebular properties and the resident OB associations. The first paper of this series (Oey & Massey 1995, hereafter Paper I) presented a numerical version of the standard model, which was applied to the superbubble DEM 152 and its stellar contents. This numerical investigation reiterated the dynamical discrepancy with the standard model found by Saken *et al.* (1992) and Brown *et al.* (1995), who used the analytic formulations. A second paper (Oey 1996a, Paper II) presented UBV photometry of the remaining 7 superbubbles in the sample, along with corresponding photometry for 5 classical H II regions for comparison. Oey (1996b, Paper III) examined the stellar contents of the superbubble sample, presenting spectral classifications, H-R diagrams, and mass functions. This fourth paper in the series will now use these stellar data to examine the dynamics of all the superbubbles and compare the standard model with the observed nebular kinematics. One final superbubble, DEM 192, is a somewhat more complex and interesting region, and will be presented in a separate paper (Oey 1996c).

2. Observational Parameters of the Superbubbles

The sample of superbubble H II regions is listed in Table 1, which provides identifications for the nebulae and stellar associations. The availability of nebular kinematic data was a primary selection criterion for the sample, and most objects also have at least limited X-ray observations. The Hα images of these superbubbles can be found in Paper III.

Table 1 also provides the radius R_s, shell thickness, ΔR, and shell density n_s for the superbubbles. These have all been determined from the Kennicutt & Hodge (1986) digitized Hα survey. As in Paper I, R_s represents the location of the shock at the outer edge of the shell, and the shell thickness represents a typical value of the FWHM of the Hα cross-section. The shell densities were also determined as in Paper I, from the emission measures EM $= \int n_e^2 dl$, where l is the column depth of emitting material and n_e is its electron density. The EM through both the shell rim and center were used to estimate n_e for each superbubble. Assuming $n_H = n_e$, the shell density n_s corresponds to n_e.

Kinematic data for these superbubbles were compiled from a variety of sources, as shown in Table 1. One uniform dataset with observations for most of the objects, are the echelle observations taken by Chu & Kennicutt (1995), who kindly provided access to their data. Additional echelle data for DEM 25 and DEM 31 were very kindly obtained and reduced by S. Points, R.C. Smith, and Y.-H. Chu in January of 1995. Both these sets of echelle data were observations of Hα taken at the CTIO 4-m. telescope. The remaining references for nebular velocities in Table 1 are from Fabry-Perot observations, mostly by Rosado and her Marseille colleagues; the only exceptions are Blades *et al.* (1980) and Dopita *et al.* (1981), who obtained kinematic data for DEM 301 with a conventional spectrograph. There are often conflicting reports in the literature for the shell expansion velocities v_s. For example, the extreme case of DEM 301 has measurements of v_s ranging from $23\,\mathrm{km\,s^{-1}}$ (Lasker 1977) to $70\,\mathrm{km\,s^{-1}}$ (Rosado *et al.* 1981). DEM 25 shows a similar range in reported kinematics between the same groups of authors. Much of this discrepancy can be explained by the different sensitivity and assumptions about velocity structure used in the different analyses, so it is important to examine how individual papers derive their reported values. Objects whose expansion velocities are marked with “:” have complex velocity structures whose v_s is not simple to assign. The shell expansion velocities given in Table 1 are best estimates based on the various available observations.

3. Superbubble Modeling

The census of the most massive stars in these superbubbles has been examined in detail and reported in Papers II and III. I will now use these data to estimate the input wind power L_w, to the superbubbles as a function of time t. These $L_w(t)$ and the observed nebular parameters can then be used to model the evolution of the superbubbles with the standard model code presented in Paper I. The $L_w(t)$ are estimated for individual stellar models computed by Schaerer *et al.* (1993), corresponding to LMC metallicity (see Paper I for details). It is then possible to sum the total $L_w(t)$ for a given stellar population.

The code for the standard model used in Paper I describes the evolution of an adiabatic, pressure-driven bubble with radiative outer shock. The evolution of $R_s(t)$ and $v_s(t)$ is then given by the solution of:

$$\frac{dR_s}{dt} = v_s \quad , \tag{1}$$

$$\frac{dv_s}{dt} = \frac{4\pi R_s^2}{M_s}\Big(P_i - P_e - \rho_0 v_s^2\Big) \quad , \tag{2}$$

and

$$\frac{dU}{dt} = L_w - P_i\frac{dV}{dt} \quad , \tag{3}$$

where M_s is the shell mass, P_i and P_e are the internal and external pressure, ρ_0 is the ambient mass density, U is the internal energy, and V is the bubble volume. These equations are then numerically integrated for the given input power $L_w(t)$. Paper I provides the details regarding the model and computation of $L_w(t)$.

Table 2 lists the numbers of massive stars currently observed in each of the superbubbles (Paper III), distributed into bins represented by the masses of Schaerer's *et al.* (1993) stellar models. Since it is likely that 1 or 2 of the most massive stars have already exploded as SNe in at least some of these associations, Table 2 also shows the original stellar population predicted by a Salpeter (1955) initial mass function (IMF). As found in Paper III, all of the resident OB associations have IMF slopes similar to Salpeter, within the errors.

The superbubble evolution models resulting from these observed stellar populations fall into two categories. The first category includes objects which exhibit the same dynamical discrepancy with the standard model that was found in Paper I for DEM 152; as discussed at length in that paper, the observed shell expansion velocity for DEM 152 is a factor of two higher than predicted by the model, and there is no simple way to reconcile the model and observations. However, in the second category of models presented here, the shell parameters are in fairly reasonable agreement with predictions. These two categories of models are shown in Figures 1 and 2. The figures show the total $L_w(t)$ (long-dashed lines) from the tabulated current stellar populations (Table 2), assuming a coeval star formation event. The resulting predicted evolution of the superbubble radius $R_s(t)$ and expansion velocity $v_s(t)$ are shown with the continuous solid and short-dashed lines, respectively. The observed R_s and v_s (Table 1) are also indicated, by the horizontal solid and short-dashed line segments. The scale for the ordinate is logarithmic for L_w, in $10\log(L_w/10^{35})$ erg s^{-1}, whereas for R_s and v_s it is linear, in pc and km s^{-1} respectively. The form of L_w is similar for all the stellar models: it consists primarily of a H-burning phase with steadily increasing wind power, followed by a sudden decrease to a red supergiant and/or luminous blue variable phase, and ending with the SN explosion. The 60 and 85 $\mathcal{M}_\odot$ models include a powerful Wolf-Rayet phase before the SN. Keeping in mind this form of the wind power evolution, one can discern in the figures the individual contributions to L_w by the various stellar mass bins; note that the models are strongly dominated by the winds of only the one or two most massive stars. The stellar data also constrain the age or time period during which we are observing the superbubble systems, in that we must be seeing them before the present stars expire as SNe. This "observation window" is denoted by the extent of the horizontal lines indicating the observed parameters.

3.1. A Dynamical Discrepancy: SN Impacts

3.1.1. Dynamical Evidence

It is clear that the models for DEM 25, 50, and 301, in the left column of Figure 1, are not consistent with the observed nebular radius and expansion velocities. In particular, the observed v_s are all at least a factor of two higher than predicted, for times corresponding to the observed R_s, so I will refer to these objects as "high-velocity" superbubbles. This is once again, the same discrepancy found in Paper I for DEM 152, and found by Saken *et al.* (1992) and Brown *et al.* (1995) for the Galactic superbubbles around Cygnus OB1 and Orion OB1. The models in Figure 1 assume a constant ambient density, such that when the shell grows to the observed R_s, it will also attain the observed shell density n_s. As discussed in Paper I, errors in the assumed density cannot reconcile the models with the observations because of the coupling between R_s and v_s through equation 1. An increase in v_s therefore requires a corresponding increase in R_s, which will only widen the discrepancy between the two at any given time. There is no simple way to account for the high shell velocity in view of the small radius. In Paper I, we also used the code to explore the possibility of ambient density gradients, which also turned out to worsen the problem.

In contrast to the high-velocity superbubbles, the models for DEM 31, 106, and 226, shown in Figure 2, are in much better agreement with the observed shell parameters. For these "low-velocity" objects, v_s is usually less than a factor of 2 discrepant at the observed R_s, and more importantly, the observed expansion velocity is actually *less* than that predicted for two of the three objects, rendering the discrepancy in the opposite sense of the high-velocity objects. It is therefore possible to explain these less prominent disagreements by invoking errors in the input wind power and/or assumed ambient density, as we shall see below. These superbubbles demonstrate that, with some adjustment in these parameters, the nebular kinematics *can* be consistent with the standard model on a detailed level, for at least some objects.

For the high-velocity objects, Paper I suggested three possibilities to explain the discrepantly small observed R_s and high v_s: (a) the ambient density has a non-spherical geometry, causing a non-spherical velocity structure such as an incipient chimney; (b) the form of the input $L_w(t)$ is substantially different; and (c) a SN blastwave(s) struck the shell, causing acceleration, in conjunction with an energy sink mechanism that inhibits shell growth. The high-velocity superbubbles examined here all have much more spherical morphologies (see images in Paper III) compared to the system studied in Paper I (DEM 152), hence (a) appears to be a less likely explanation. For (b), the most credible possibility is an alteration of the stellar population, or non-coeval age distribution for the stars. Paper I demonstrated that this is highly unlikely to resolve the problem; however, it is worth reexamining this possibility for these new objects.

The models in the right column of Figure 1 are the same as those on the left, but now including the few, additional high-mass stars predicted by a Salpeter IMF (Table 2). The inclusion of these stars greatly narrows the observation window, since the minimum age of the superbubble is now also constrained by the absence of the inferred stars. The models including these stars confirm the finding in Paper I, that the inclusion of additional high-mass stars cannot reconcile the models with the observations.

I shall now relax the assumption of coeval star formation. Shull & Saken (1995) show that differences in the star formation rate will significantly affect the form of the input power with time, even during the stellar wind-dominated period. The H-R diagrams for DEM 25 and DEM 50 (Fig. 5 in Paper III) show the presence of one or two noticeably evolved, high-mass stars to the right of the main sequence. The models in Figure 1 are therefore not strictly compatible with the observations, since they assume that the entire population was born simultaneously (provided that the evolved stars are not foreground or background field stars). Schaerer's *et al.* (1993) evolutionary models indicate an age of 9.12 Myr for the evolved $20\,\mathcal{M}_\odot$ star in DEM 25. The left side of Figure 3 now shows the superbubble model for DEM 25, assuming this $20\,\mathcal{M}_\odot$ star was born 6 Myr before the rest of the currently observed stars. Similarly, the H-R diagram for DEM 50 shows one $20\,\mathcal{M}_\odot$ star and one $40\,\mathcal{M}_\odot$ star, with inferred ages of 9.13 and 4.82 Myr, respectively. Figure 3 also shows the superbubble model for DEM 50, with the $20\,\mathcal{M}_\odot$ star born at $t = 0$, followed by the $40\,\mathcal{M}_\odot$ star at $t = 4.31$ Myr, and finally the remainder of the currently observed stars at $t = 6$ Myr. It is apparent in Figure 3 that changing the star formation sequence also cannot resolve the discrepancy with the standard model. In particular, the shell expansion velocity cannot be reproduced, especially while maintaining the observed R_s. The models in Figure 3 do not include the additional, predicted high-mass stars, but since R_s is already within the observed range during the observation window, any additional high-mass stars would clearly cause R_s to blow up far beyond the observed value, especially if it were possible to match v_s. This confirms the results in Paper I, that changing the stellar population and star formation sequence cannot reconcile the observations of the shell kinematics to the standard model.

The remaining possibility for explaining the dynamical discrepancy is therefore (c), that a SN blastwave has struck the superbubble shell, accelerating it, while some factor simultaneously inhibits the growth of the shell. Although the $L_w(t)$ formulated here do include SN explosions, these are simply treated as enhancements in the continuous wind injection. As discussed in Paper I, this implies that the SN energy is thermalized at the inner, reverse shock, whereas in reality, the supersonic blastwave could reach the shell. It is clear in Figure 1 that the inferred high-mass stars that presumably lead to these SNe should cause all the superbubbles to grow much larger than is currently observed. This would either require a growth-rate discrepancy in the standard model, or some additional factor is to reduce the pre-SN growth. Although these issues render option (c) bit awkward at first glance, I show below in §3.2 that evidence is indeed pointing in the direction of a growth-rate discrepancy.

3.1.2. Observational Evidence for SNR Impacts

As mentioned above, Chu & Mac Low (1990) and Wang & Helfand (1991) found an excess in the observed X-ray luminosities of several superbubbles. Both papers suggested that the excess emission is due to SNRs striking the shell walls. Chu & Mac Low (1990) demonstrated numerically that such an impact can easily provide an order of magnitude enhancement in the X-ray luminosity, although the specific increase is quite sensitive to the distance of the SN from the shell and the detailed density structure within the superbubble and shell. In the meantime, Chu *et al.* (1995) have also identified a number of superbubbles which do not display excess X-ray emission, and have luminosity limits consistent with the predictions of the standard model. If the X-ray bright objects are explained by SNR impacts, the X-ray dim objects would presumably be superbubbles with no recent SNR heating.

Table 3 shows the observed X-ray luminosities of the superbubbles in the sample, divided into the high-velocity objects that are dynamically inconsistent with the standard model as found in the preceding section, and low-velocity objects that appear to be dynamically consistent with the model. Without exception, Table 3 shows that the two dynamical categories of superbubbles correspond exactly to the X-ray bright and X-ray dim categories. Among the X-ray bright superbubbles, DEM 301 was detected by *EINSTEIN* and appeared in the Chu & Mac Low (1990) and Wang & Helfand (1991) investigations reporting X-ray excess in superbubbles. *ROSAT* luminosities for DEM 25 and DEM 50 have been kindly provided by K. Dennerl, and Table 3 shows that these superbubbles also have X-ray luminosities $L_x > 1\times 10^{35}\ \mathrm{erg\,s^{-1}}$. In the X-ray dim category, DEM 31 and 106 both appeared in the Chu *et al.* (1995) *ROSAT* study of X-ray dim superbubbles, and *ROSAT* observations of the area including DEM 226 visually show no evidence of X-ray detection (Y.-H. Chu, private communication).

The X-ray luminosity L_x in the 0.1–2.4 keV *ROSAT* bandpass is predicted by

$$L_x = 6.6\times 10^{27} n_0^{10/7} R_s^{17/7} v_s^{16/7}\ \mathrm{erg\,s^{-1}} \tag{4}$$

(Chu *et al.* 1995), assuming a metallicity of 0.4 relative to solar. Approximating that a constant original ambient density n_0 has been swept into a shell of thickness ΔR, it is possible to infer n_0

by

$$n_0 \simeq 3\left(\frac{\Delta R}{R_s}\right) n_s \quad . \tag{5}$$

However, equation 4 is derived directly from the standard model's analytic expressions. Since these expressions are not valid for the high-velocity superbubbles, the predicted L_x derived from equation 4 will be grossly overestimated due to the much larger observed value of v_s relative to R_s in these objects.

For the high-velocity objects, X-ray predictions consistent with the standard model can be made by estimating the value for v_s that would be expected, had these high-velocity superbubbles followed the model evolution. Based on the models on the right side of Figure 1, Table 3 also shows the predicted v_s for the observed R_s of the high-velocity superbubbles. Note that these v_s are still likely to be overestimates, since the predicted shell radii grow much faster than the observations imply (Figure 1). For the high-velocity superbubbles, the expected X-ray luminosities based on these predicted expansion velocities are shown in Table 3, along with the derived ambient densities and predicted v_s. For the low-velocity objects, L_x is computed from the observational v_s, and also tabulated in Table 3.

The values of L_x based on the expected values of v_s imply an X-ray enhancement in the high-velocity superbubbles, contrasting with the X-ray dim objects. While adoption of the predicted v_s vs. the observed v_s renders the calculation of L_x rather speculative, it is nevertheless meaningless to use the observed v_s in equation 4 for these high-velocity objects, since the kinematics have diverged from the standard model. Regardless of the predicted luminosities, however, the observed values of L_x in Table 3 show a correspondence with the dynamical partition.

Table 3 also lists the [S II]/Hα ratios for the sample. Most of these ratios were measured by Lasker (1977). There are no measurements for DEM 106 and DEM 226, but the large-scale, narrow-band images of the LMC taken by Lasker (1979) show that the [S II]/Hα ratio for these objects is less than that for DEM 301, and perhaps similar to that for DEM 31. The [S II]/Hα ratios in Table 3 also fall neatly into the bimodal partition: objects with [S II]/H$\alpha \gtrsim 0.5$ correspond to the high-velocity, X-ray bright superbubbles, while the low-velocity, X-ray dim superbubbles exhibit lower values. The high [S II]/Hα ratios again suggest recent shock heating in the high-velocity superbubbles, plausibly by SNRs, although other mechanisms are possible.

Previously studied superbubbles also fit these patterns. DEM 152, as shown in Paper I, is also a high-velocity ($v_s \sim 35 - 40\ \mathrm{km\,s^{-1}}$), X-ray bright object. The mean [S II]/Hα ratio from 28 measurements of the main shell reported by Hunter (1994) is 0.46. Similarly, the Orion-Eridanus X-ray enhancement was one of the earliest identifications of X-ray emission from a superbubble (Reynolds & Ogden 1979), being linked to the Orion OB 1 association. The shell turns out to have a high expansion velocity ($v_s \sim 30 - 40\ \mathrm{km\,s^{-1}}$) and is also a dynamically discrepant object (Brown *et al.* 1995). Burrows *et al.* (1993) and Reynolds & Ogden (1979) have already suggested that its X-ray emission can be explained by a wind-blown bubble with possible reheating by SNe.

If the hot gas is centered on the Orion OB 1 association (though its centroid could be nearer), the inferred $L_x = 6.3 \times 10^{35}$ erg s^{-1} (Burrows *et al.* 1993) in the 0.1–1.0 keV *HEAO-1* A-2 bandpass. This luminosity is already well within the range of X-ray bright objects, even without correcting to the broader 0.1–2.4 keV *ROSAT* bandpass.

There is thus a clear correspondence between the strong X-ray and [S II] emission, and the high-velocity superbubbles whose dynamics are inconsistent with the standard model. Likewise, the superbubbles that show no signatures of SN activity remain consistent with the model. Finally, it is also apparent that the high-velocity objects all show a lack of high-mass stars compared to the low-velocity systems (Table 2), as would be expected with the loss of high-mass stars as SN progenitors. Hence, these factors all suggest a hypothesis of SNR impacts to explain the deviations from the model. The discrepantly high expansion velocities would then result from acceleration due to the SNR collision with the shell. From 2-D simulations of such collisions, Tenorio-Tagle *et al.* (1991) find that the shells gain a kinetic energy contribution of $0.1 - 0.3\ E_{sn}$ (Franco *et al.* 1991), where E_{sn} is the supernova energy, $\sim 1 \times 10^{51}$ erg. According to this estimate, an SNR uniformly colliding with a $10^4\,\mathcal{M}_\odot$ shell with an initial $v_s \sim 15$ km s^{-1} yields a new expansion velocity of ~ 47 km s^{-1} (Paper I). For the high-velocity superbubbles, which have shell masses ranging from $1 - 3 \times 10^4\,\mathcal{M}_\odot$, their observed $25 - 60$ km s^{-1} range in v_s is easily consistent with these estimates, especially given that the acceleration is naturally dependent on the specific geometry and other parameters. It is clear that the observations are energetically consistent with SNR acceleration.

3.2. A Growth Rate Discrepancy

Returning now to the low-velocity superbubbles, Figure 2 shows that the observed expansion velocities are actually higher than predicted for two of the three objects. The left column of Figure 4 shows the models for the low-velocity superbubbles with L_w/n_0 reduced by a factor of 10. For DEM 106 and DEM 226, the observational parameters are now completely consistent with the models, both in terms of v_s and R_s simultaneously agreeing, and furthermore agreeing within the permitted observation window. These models demonstrate the possible dynamical validity of the standard model, although a scalar adjustment appears to be necessary.

The outstanding problem in these low-velocity objects is the apparently large overestimate in effective L_w/n_0. However, as detailed in the previous section, the inferred SN progenitors in the high-velocity superbubbles also imply a substantial overestimate in predicted R_s for those objects (Figure 1,right col.). It therefore appears that this is a general problem with the application of the standard model in *both* categories of objects, and I will refer to this as the shell "growth rate discrepancy." The right column of Figure 4 shows the models for the high-velocity superbubbles, now also with L_w/n_0 reduced by a factor 10. These are otherwise the same as the models seen on the right side of Figure 1. It is remarkable that, in keeping with our hypothesis of SNR acceleration, these models now also show a predicted R_s that is consistent with the observations, at the time of the first SN explosion! This time is indicated by the vertical dotted line in Figure 4. The pattern suggests that SNR impacts might be catalysts for some process inhibiting further shell growth.

The astute reader will notice that the overestimate in predicted growth rate apparently does not apply to DEM 31. However, this object is a somewhat more complicated system. The putative $120\,\mathcal{M}_\odot$ star is Br 5, a WN6-A star, discussed in §2.2.1 and §3.3 of Paper III. Its initial mass, like those of any Wolf-Rayet star, is highly uncertain, and the evolution of the superbubble is strongly dependent on its mass. The morphology of DEM 31 itself is the most asymmetric of the sample, and Br 5, along with the rest of the OB association LH 6, is located very close to the south side of the shell, and not in the center as one might expect. Furthermore, the shell does not appear whole, and exhibits a possible blowout on the northeast side. As indicated in Table 1, the velocity structure of this superbubble is complex. It is therefore unclear how the kinematics of this system are related to the bimodal pattern found in the rest of the sample.

Thus with the sole exception of DEM 31, both the low-velocity and high-velocity objects suggest a sizeable overestimate in effective input power. The observations and reduced L_w/n_0 models are *simultaneously* consistent in the three parameters: R_s, v_s, and observation time, for all but one of the six objects. This strongly suggests the existence of a discrepancy in the shell growth rate with the standard model.

In addition, a similar order-of-magnitude discrepancy in effective input power compared to observed nebular kinematics was identified over a decade ago by Treffers & Chu (1982) for bubbles of Wolf-Rayet stars. More recently, García-Segura & Mac Low (1995) arrived at the same conclusion in their detailed study of the Wolf-Rayet bubble NGC 6888, which exhibits this energetic discrepancy with their analytic models. These authors also found radiative cooling an unlikely agent, and García-Segura & Mac Low suspect an order of magnitude overestimate in L_w of the central star, despite direct observational measurements of the wind parameters. In addition, Drissen *et al.* (1995) also identify this energetic discrepancy in a small bubble containing 3 Wolf-Rayet stars in NGC 3603. They estimate over an order of magnitude disagreement in the inferred L_w to the bubble. This growth rate discrepancy is thus appearing in both superbubbles and the single-star bubbles of Wolf-Rayet stars.

3.2.1. Possible Alternatives

However, alternative explanations must also be considered. The inference of an order of magnitude growth rate discrepancy is based on two factors: first, the observed R_s of the high-velocity shells are apparently too small to accommodate a SN progenitor; and second, the observed v_s of the two, "clean" low-velocity shells are apparently too high. If both factors are in error, this growth rate discrepancy may not exist. The first factor could be dismissed by the rejection of the SNR impact hypothesis. Even with the occurrence of SNR impacts, the first factor can be avoided with the implausible, but possible, scenario discussed next, in which a single lower-mass SN progenitor dominated the shell formation, with the remainder of the association born later, thus dynamically unimportant to the shell. The second factor above can be avoided if the masses of the most luminous stars in DEM 106 and DEM 226 have been overestimated by one stellar mass track: I assigned masses from the set of of Schaerer's *et al.* (1993) evolutionary tracks, and although the positions on the H-R diagram are fairly robust for stars with spectral types, it is possible that a slightly different stellar model is more appropriate (see, *e.g.,* Paper III). The initial mass of the most luminous star in DEM 106, in particular, is more uncertain since it is the B[e] supergiant S22. Likewise, if blowouts perpendicular to the line of sight have actually occurred in DEM 106 and DEM 226, the shells may be stalled, and the observed v_s would be lower than expected. This may be suggested by the nebular morphology of DEM 106, although not by DEM 226. Thus, it may be possible, through erroneously concluding that the high-velocity shells are too small, *and* that the low-velocity shells are expanding too slowly, that there may be no growth rate discrepancy with the standard model as currently applied.

However, assuming the observed parameters are essentially correct, it may be remotely possible to reconcile the observations with the models as follows. For the high-velocity superbubbles, the coincidence of the observed and predicted shell radius at the time of the first SN relies on the extrapolation of the expected high-mass stars from a Salpeter IMF (Table 2). Another, but unlikely, possibility is that one or two lower-mass stars, perhaps 15–20 $\mathcal{M}_{\odot}$, were the primary agents generating the superbubble, with the accelerated shell resulting from the SN of one of these. This scenario requires that the superbubble be $\gtrsim$ 10 Myr old in order for the SN explosion to occur. It also implausibly requires that all of the remaining high-mass stars in the observed OB association were born recently, within the last 3 or 4 Myr, and are dynamically unimportant for the shell growth. Otherwise, the stellar winds from these stars would again have caused the shell radius to be larger than currently observed. The models in Figure 3 can be used to demonstrate this scenario, with a single 20 $\mathcal{M}_{\odot}$ star responsible for the shell growth over most of its lifetime, and the rest of the association born 6 Myr later. It is apparent that R_s is already at least 50 pc by the time of the first SN explosion. For the superbubbles studied here, the mass of the isolated, precursor stars responsible for the shell growth cannot exceed 20–25 $\mathcal{M}_{\odot}$, and again, all the currently observed high-mass stars must be energetically unimportant. It would seem extremely unlikely that the observed groups of high-mass stars seen in almost all superbubbles (*e.g.,* Paper III; Braunsfurth & Feitzinger 1983; Rosado 1986) are irrelevant to the growth of the shell.

Thus the simplest conclusion remains that there is a discrepancy in equivalent effective L_w/n_0 to the superbubbles. Although Figure 4 shows L_w/n_0 reduced by an order of magnitude, a factor of several could bring the models within comfortable range of the observational parameters. I will now consider possible explanations for such an effect.

3.2.2. Possible Causes

The following, or a combination of these factors, could be responsible for the apparent growth rate discrepancy.

1. The assumed shell thickness and density, and thereby the ambient density, could be underestimated. However, the ionizing fluxes of these OB associations make it unlikely that a substantial neutral shell exists around these superbubbles. Even for DEM 25, the object with the coolest stars, the implied Strömgren sphere should be 30% larger than the radius of the shell. Meaburn *et al.* (1984) also found no evidence of corresponding H I expanding shells for four of the objects in this sample, although it should be noted that their beam size was larger than these objects. But as described in Paper I, more than tripling the assumed shell thickness to account for a neutral component, will cause $< 20\%$ deviation in the growth of R_s for an observed radius of 30 pc. Still, resolved H I mapping of the superbubble environment is desirable to further constrain this issue.

2. Several authors (*e.g.,* Shull & Saken 1995; Weaver *et al.* 1977) discuss the potential importance of radiative cooling as an energy-loss mechanism. This process has been thought to take place primarily in the interface between the hot superbubble interior and the cool shell, where the temperatures are predicted to range from $10^5 - 10^6$K. Since the cooling curve favors UV emission, most of this radiation could occur at those wavelengths (*e.g.,* Weaver *et al.* 1977). It is worth noting that cooling by soft X-ray emission from the hot interior of the bubble, as discussed by *e.g.,* Shull & Saken (1995) and Martin & Kennicutt (1995) does not appear to be a significant energy-loss mechanism in these objects. A comparison of Table 3 with Figure 2 for the pre-SN superbubbles shows that the observed X-ray luminosity is 1–2 orders of magnitude or more, below the inferred L_w.

3. As discussed in Paper I, the assumptions for the wind power of individual dominant stars could be uncertain to even an order of magnitude, although it seems hard to believe that the estimates for the entire sample are overestimated by such a large factor. In the models presented above, the mass-loss rates $\dot{M}$ used to estimate L_w are the same as those adopted by Schaerer *et al.* (1993) in the stellar models, and are scaled for LMC metallicity. Since the evolutionary tracks are quite sensitive to the adopted $\dot{M}$, a self-consistent formulation for $L_w(t)$ based on these models required adoption of these same $\dot{M}$. The $\dot{M}$ have been scaled with metallicity as $(Z/\mathrm{Z}_\odot)^{0.5}$, which appears to be consistent with the available observations in the Magellanic Clouds (*e.g.,* Garmany & Conti 1985; Leitherer 1988; Garmany & Fitzpatrick 1988). The terminal wind velocities v_∞ have been computed with the empirical parameterizations of Howarth & Prinja (1989) for Galactic O stars, and have not been adjusted for LMC metallicity. The predicted lower v_∞ could account for an overestimate in L_w by a factor of 0.25–0.5, although the observed v_∞ for the hottest stars appear comparable to those in the Galaxy (Walborn *et al.* 1995).

Lamers & Leitherer (1993) and Castor (1993) discuss the high degree of uncertainty in mass-loss rates for massive stars. In particular, Castor points out that the parameterizations of de Jager *et al.* (1988) which are used by Schaerer *et al.* (1993), may assume too much variation in $\dot{M}$ during the H-burning phase, which can vary by an order of magnitude or more. Also, Moffat & Robert (1994) provide evidence that the measurements themselves, of $\dot{M}$ derived from radio observations of Galactic stars, could be overestimated by a factor of $\gtrsim 3$, which would improve agreement with the bubble models.

Naturally, all of the above factors could conspire to produce the implied growth rate discrepancy. Finally, it should be noted that if the superbubbles are actually non-adiabatic, the adiabatic standard model used here would not apply. Instead, we would expect a momentum-conserving model (*e.g.,* Steigman, Strittmatter, & Williams 1975) or a partially-radiative bubble model (Koo & McKee 1992a, b). But whatever the actual reason(s), the superbubble growth rate seems to be less than predicted by the standard model, using stellar winds as parameterized here.

4. Conclusion

It is apparent that for the high-velocity superbubbles, SN impacts can cause a major deviation from the model predictions. High-velocity superbubbles with $v_s \gtrsim 25$ km s^{-1} are very common, with about as many of these known as the low-velocity objects (*e.g.,* Rosado 1986). The models in §3 demonstrate that it is essentially impossible to obtain expansion velocities $\gtrsim 25$ km s^{-1} in superbubbles with radii of a few tens of pc without acceleration by the presumed SNR impacts. Since these post-impact superbubbles are so commonplace, it is vital to better understand the role these SNRs play in their evolution. Do these impacts permanently disrupt the shell structure with the expected Rayleigh-Taylor instabilities seen in the simulations of *e.g.,* Tenorio-Tagle *et al.* (1991)? It seems possible; for example, DEM 152 shows large quantities of hot, X-ray–emitting gas leaking out of the superbubble through just such a blowout feature (Chu *et al.* 1993; Magnier *et al.* 1995), presumably depressurizing the bubble. If SNR impacts in superbubbles are commonplace, as suggested by the numbers of high-velocity objects, this could possibly imply that coronal gas is released into low-density pockets of the ISM. The fate of the shells and their content depends on the exact nature of the ambient environment.

It is also worth noting that, while the complicated form of $L_w(t)$ during massive star evolution already limits the utility of the standard model's analytic formulations in computing superbubble parameters such as age, the large deviations from the model render such formulations virtually inapplicable in the high-velocity objects. Indeed, the typical anticipated lifetime of superbubble growth is now several times shorter than previous estimates of $\gtrsim 10$ Myr, which were determined by the ambient interstellar pressure or termination of the stellar winds. In the picture implied here, shell disruption probably occurs with the explosion of the first SNe of the parent association, at ages of ~ 3 Myr. Therefore, analytic expressions must be applied with great care if used to derive superbubble parameters.

In summary, I have used the census of the enclosed stellar populations (Papers II, III) to estimate the wind power $L_w(t)$ input to these superbubbles, and model their dynamical evolution as predicted by the Weaver *et al.* (1977) model. The results are as follows:

(1) There are two categories of superbubbles in the sample: the "high-velocity" superbubbles, which are dynamically inconsistent with the standard model, such that the expansion velocities are too high for the observed radii; and the "low-velocity" objects, which are essentially dynamically consistent with the model.

(2) Elevated X-ray emission in the high-velocity superbubbles suggests acceleration by SNR impacts to explain their anomalous dynamics.

(3) Both categories of superbubble models predict much faster shell growth than can be accounted for with the observations. This implies one or more of the following factors: an overestimate in the input wind power, an identical underestimate in the ambient density, and/or an energy sink mechanism. The discrepancy is the equivalent of up to an order of magnitude reduction in effective input power.

I am happy to thank John Bieging, Adam Burrows, You-Hua Chu, Rob Kennicutt, and Mordecai Mac Low for helpful discussions. My gratitude also to Y.-H. Chu, Sean Points, and Chris Smith for obtaining echelle data, and Dominik Bomans and Konrad Dennerl for access to X-ray data in advance of publication. I also thank the anonymous referee for helpful comments that improved this paper. This work was supported by a predoctoral American Fellowship of the American Association of University Women, the University of Arizona Graduate College, and NSF grants AST90-19150 and AST94-21145.

TABLE 1

OBSERVED SUPERBUBBLE PARAMETERS[a]

DEM	Henize	LH	R_s (pc)[b]	ΔR (pc)[b]	n_s (cm^{-3})[c]	v_s ($km\,s^{-1}$)[d]	Reference[e] for v_s
25	N185	···	43	2.5	6.5	60:	This work, Rosado *et al.* (1982), L77
31	N9	6	50	5	4.0	30:	This work, CK, L93, G83
50	N186 CE	···	50	6	4.0	25	CK, Rosado *et al.* (1990), L77
106	N30 BC	38	30	6	5.5	$\lesssim 10$	CK
226	N148 GI	73	28	7	4.5	$\lesssim 5$	CK
301	N70	114	53	4	6.5	40:	CK, Dopita *et al.* (1981), Rosado *et al.* (1981), Blades *et al.* (1980), G83, L77

[a]Identifications: DEM = Davies, Elliott, & Meaburn 1976; N = Henize (1956); LH = Lucke & Hodge (1970).
[b]Uncertainty $\sim 10-15\%$.
[c]Uncertainty $\sim 30\%$.
[d]Objects with ":" uncertain to 50%, but see text; others $\sim 20\%$.
[e]CK = Chu & Kennicutt (1995)
G83 = Georgelin *et al.* (1983)
L77 = Lasker (1977)
L93 = A. Laval, as quoted in Chu *et al.* (1995)
This work = new data kindly obtained by S. Points, R.C. Smith, & Y.-H. Chu

Table 2. Stellar Population Models[a]

DEM	120 $\mathcal{M}_\odot$ $\tau = 3.12$	85 $\mathcal{M}_\odot$ $\tau = 3.48$	60 $\mathcal{M}_\odot$ $\tau = 4.12$	40 $\mathcal{M}_\odot$ $\tau = 5.26$	25 $\mathcal{M}_\odot$ $\tau = 7.84$	20 $\mathcal{M}_\odot$ $\tau = 9.96$	15 $\mathcal{M}_\odot$ $\tau = 14.2$	12 $\mathcal{M}_\odot$ $\tau = 19.58$
High-velocity superbubbles[b]								
25	0	0	0 (1)	0 (1)	2	2	2	8
50	0	0 (1)	0 (1)	3	1	7	6	9
301	0	0	0 (1)	3	3	1	4	2
Low-velocity superbubbles								
31	1	0	0	1	4	2	1	3
106	0	1	0	2	0	4	1	3
226	0	0	1	1	0	1	2	1

[a]Table represents numbers of stars in each mass bin. The stellar model lifetime in Myr is also shown in the column heading.

[b]Values in parentheses show inferred original number of stars based on a Salpeter IMF.

Table 3. X-ray Luminosities and [S II]/Hα Ratios

DEM	Observed L_x[a] (10^{35} erg s^{-1})	[S II]/Hα[b]	n_0 (cm^{-3})	Predicted L_x (10^{35} erg s^{-}1)	Predicted v_s (km s^{-1})
		High-velocity superbubbles			
25	1.8 (1)	0.64	1.1	0.34	15
50	4.2 (1)	$\sim$ 1.	1.4	1.3	20
301	5.4 (2)	0.52	1.5	0.76	14
		Low-velocity superbubbles			
31	$\lesssim$ 1.0 (3)	0.29	1.2	2.7	...
106	$<$ 0.9 (3)	$<$ 0.4[c]	3.3	0.3	...
226	(see text) (4)	$<$ 0.4[c]	3.4	0.05	...

[a] References for X-ray luminosities shown by numbers in parentheses:
(1) K. Dennerl, private communication
(2) Chu & Mac Low (1990); scaled by factor of 3 to adjust to *ROSAT* bandpass
(3) Chu *et al.* (1995)
(4) Y.-H. Chu, private communication

[b] From Lasker (1977), unless otherwise indicated.

[c] Visually estimated from images in Lasker (1979).

REFERENCES

Abbott, D. C. 1982, ApJ, 263, 723

Arthur, S. J. & Henney, W. J. 1995, ApJ, in press

Blades, J. C., Elliott, K. H., & Meaburn, J. 1980, MNRAS, 192, 101

Braunsfurth, E., & Feitzinger, J. V. 1983, A&A, 127, 113

Brown, A. G. A., Hartmann, D., & Burton, W. B. 1995, A&A, submitted

Burrows, D. N., Singh, K. P., Nousek, J. A., Garmire, G. P., & Good, J. 1993, ApJ, 406, 97

Castor, J. I., McCray, R., & Weaver, R. 1975, ApJ, 200, L107

Castor, J. I. 1993, in *Massive Stars: Their Lives in the Interstellar Medium,* J. P. Cassinelli & E. B. Churchwell, eds., (San Francisco: Astron. Soc. Pacific), 297.

Chu, Y.-H., Chang, H.-W., Su, Y.-L., & Mac Low, M.-M. 1995, ApJ, in press

Chu, Y.-H. & Kennicutt, R. C. 1995, in preparation

Chu, Y.-H. & Mac Low, M.-M. 1990, ApJ, 365, 510

Chu, Y.-H., Mac Low, M.-M., García-Segura, G., Wakker, B., & Kennicutt, R. C. 1993, ApJ, 414, 213

Davies, R. D., Elliott, K. H., & Meaburn, J. 1976, *Mem.R.A.S.* 81, 89

de Jager, C., Niewenhuijzen, H., & van der Hucht, K. A. 1988, A&AS, 72, 259

Dopita, M. A., Ford, V. L, McGregor, P. J., Mathewson, D. S., & Wilson, I. R. 1981, ApJ, 250, 103

Drissen, L., Moffat, A. F. J., Walborn, N. R., & Shara, M. R. 1995, AJ, in press

Franco, J., Tenorio-Tagle, G., Bodenheimer, P., & Różyczka, M. 1991, PASP, 103, 803

García-Segura, G. & Mac Low, M.-M. 1995, ApJ, submitted

Garmany, C. D. & Conti, P. S. 1985, ApJ, 293, 407

Garmany, C. D. & Fitzpatrick, E. L. 1988, ApJ, 332, 711

Georgelin, Y. M., Georgelin, Y. P., Laval, A. , Monnet, G., & Rosado, M. 1983, A&AS, 54, 459

Henize, K. G. 1956, ApJS, 2, 315

Howarth, I. D. & Prinja, R. K. 1989, ApJS, 69, 527

Hunter, D. A. 1994, AJ, 107, 565

Kennicutt, R. C. & Hodge, P. W. 1986, ApJ, 306, 130

Koo, B.-C. & McKee, C. F. 1992a, ApJ, 388, 93

Koo, B.-C. & McKee, C. F. 1992b, ApJ, 388, 103

Lamers, H. J. G. L. M. & Leitherer, C. 1993, ApJ, 412, 771

Lasker, B. M. 1977, ApJ, 212, 390

Lasker, B. M. 1979, Contr. Cerro-Tololo Inter-American Obs., 127

Leitherer, C. 1988, ApJ, 334, 626

Lucke, P. B. & Hodge, P. W. 1970, AJ, 75, 171

Mac Low, M.-M. & McCray, R. 1988, ApJ, 324, 776

Magnier, E. A., Chu, Y.-H., Points, S. D., Hwang, U., & Smith, R. C. 1995, ApJ, submitted

Martin, C. L. & Kennicutt, R. C. 1995, ApJ, 447, 171

Massey, P, Garmany, C. D., Silkey, M., & Degioia-Eastwood, K. 1989a, AJ, 97, 107

Massey, P., Parker, J. W., & Garmany, C. D. 1989b, AJ, 98, 1305

McKee, C. F., Van Buren, D., & Lazareff, B. 1984, ApJ, 278, L115

Meaburn, J., McGee, R. X., & Newton, L. M. 1984, MNRAS, 206, 705

Moffat, A. F. J. & Robert, C. 1994, ApJ, 421, 310

Oey, M. S. 1996a, ApJS, in press (Paper II)

Oey, M. S. 1996b, ApJ, in press (Paper III)

Oey, M. S. 1996c, in preparation

Oey, M. S. & Massey, P. 1995, ApJ, 452, 210 (Paper I)

Reynolds, R. J. & Ogden, P. M. 1979, ApJ, 229, 942

Rosado, M. 1986, A&A, 160, 211

Rosado, M., Georgelin, Y. P., Georgelin, Y. M., Laval, A., & Monnet, G. 1981, A&A, 97, 342

Rosado, M., Georgelin, Y. P., Georgelin, Y. M., Laval, A., & Monnet, G. 1982, A&A, 115, 61

Rosado, M., Laval, A., Boulesteix, J., Georgelin, Y. P., Greve, A., Marcelin, M., Le Coarer, E., & Viale, A. 1990, A&A, 238, 315

Saken, J. M., Shull, J. M., Garmany, C. D., Nichols-Bohlin, J., & Fesen, R. A. 1992, ApJ, 397, 537

Salpeter, E. E. 1955, ApJ, 121, 161

Schaerer, D., Meynet, G., Maeder, A., & Schaller, G. 1993, A&AS, 98, 523

Shull, J. M. & Saken, J. M. 1995, ApJ, 444, 663

Steigman, G., Strittmatter, P. A., & Williams, R. E. 1975, ApJ, 198, 575

Tenorio-Tagle, G., Różyczka, M., Franco, J., & Bodenheimer, P. 1991, MNRAS, 251, 318

Treffers, R. R. & Chu, Y.-H. 1982, ApJ, 254, 569

Walborn, N. R., Lennon, D. J., Haser, S. M., Kudritzki, R.-P., & Voels, S. A. 1995, PASP, 107, 104

Wang, Q. & Helfand, D. J. 1991, ApJ, 373, 497

Weaver, R., McCray, R., Castor, J., Shapiro, P., Moore, R. 1977, ApJ, 218, 377

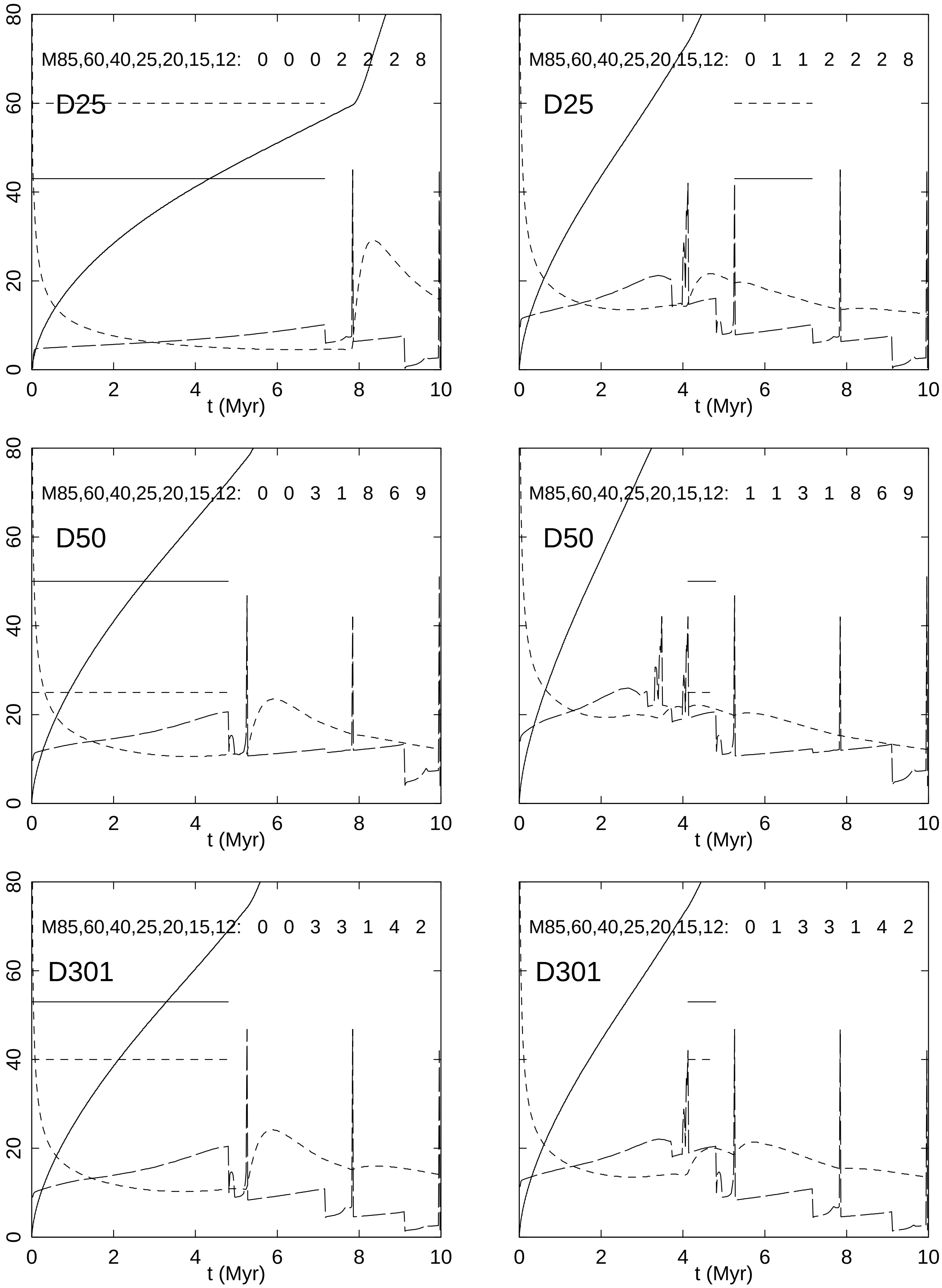

Fig. 1.— Models for high-velocity superbubbles. Continuous lines represent input L_w in $10 \log L_{35}$ (long-dashed), and resultant $R_s(\mathrm{pc})$ (solid) and $v_s(\,\mathrm{km\,s^{-1}})$ (short-dashed). The horizontal line segments correspond to observed R_s (solid) and v_s (short-dashed), with extent of the segments indicating the permitted observation window (see text). Models on left are for L_w computed from the currently observed massive star population, and on right for the original population predicted by a Salpeter IMF. The stellar census is shown at the top of each model.

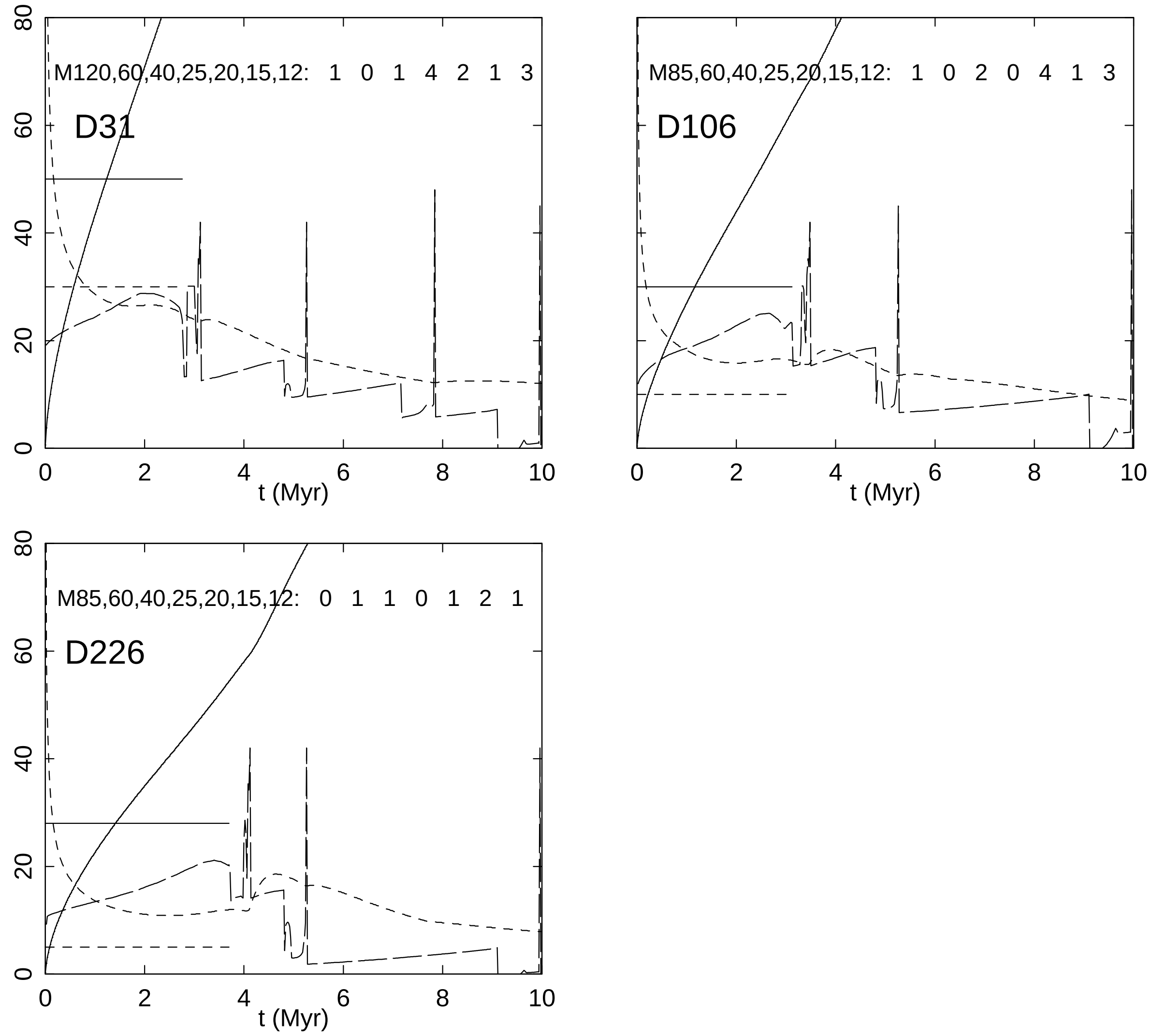

Fig. 2.— Superbubble models for low-velocity superbubbles. Note the highest mass star for DEM 31 is $120\,\mathcal{M}_{\odot}$, not $85\,\mathcal{M}_{\odot}$.

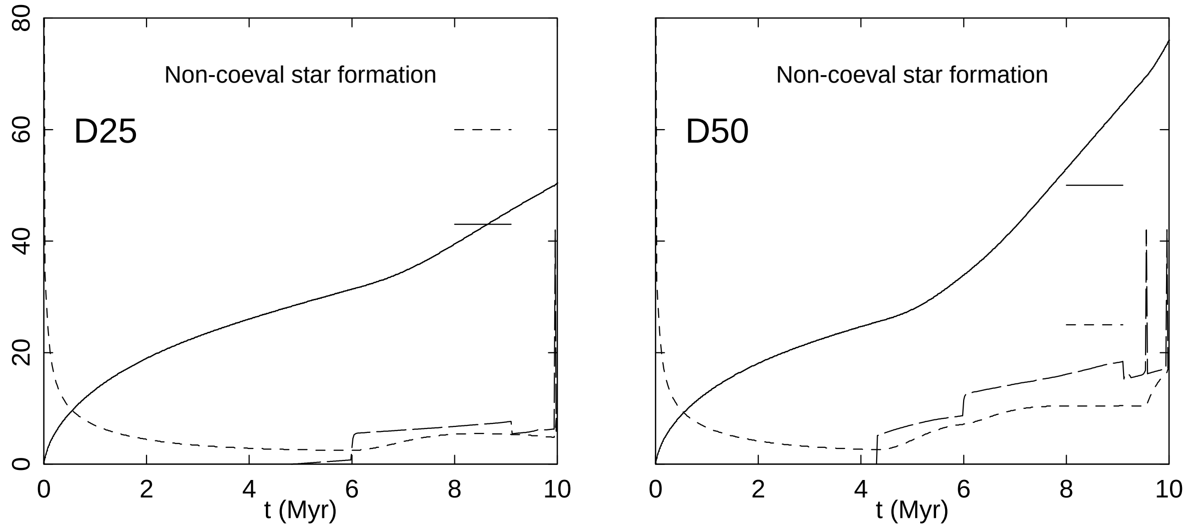

Fig. 3.— Models for DEM 25 and DEM 50, relaxing the assumption of coeval star formation. The formation of the OB association at 6 Myr is preceded by a $20\,\mathcal{M}_\odot$ star in DEM 25, and by a $20\,\mathcal{M}_\odot$ and $40\,\mathcal{M}_\odot$ star in DEM 50 (see text). Line types are same as in Figure 1.

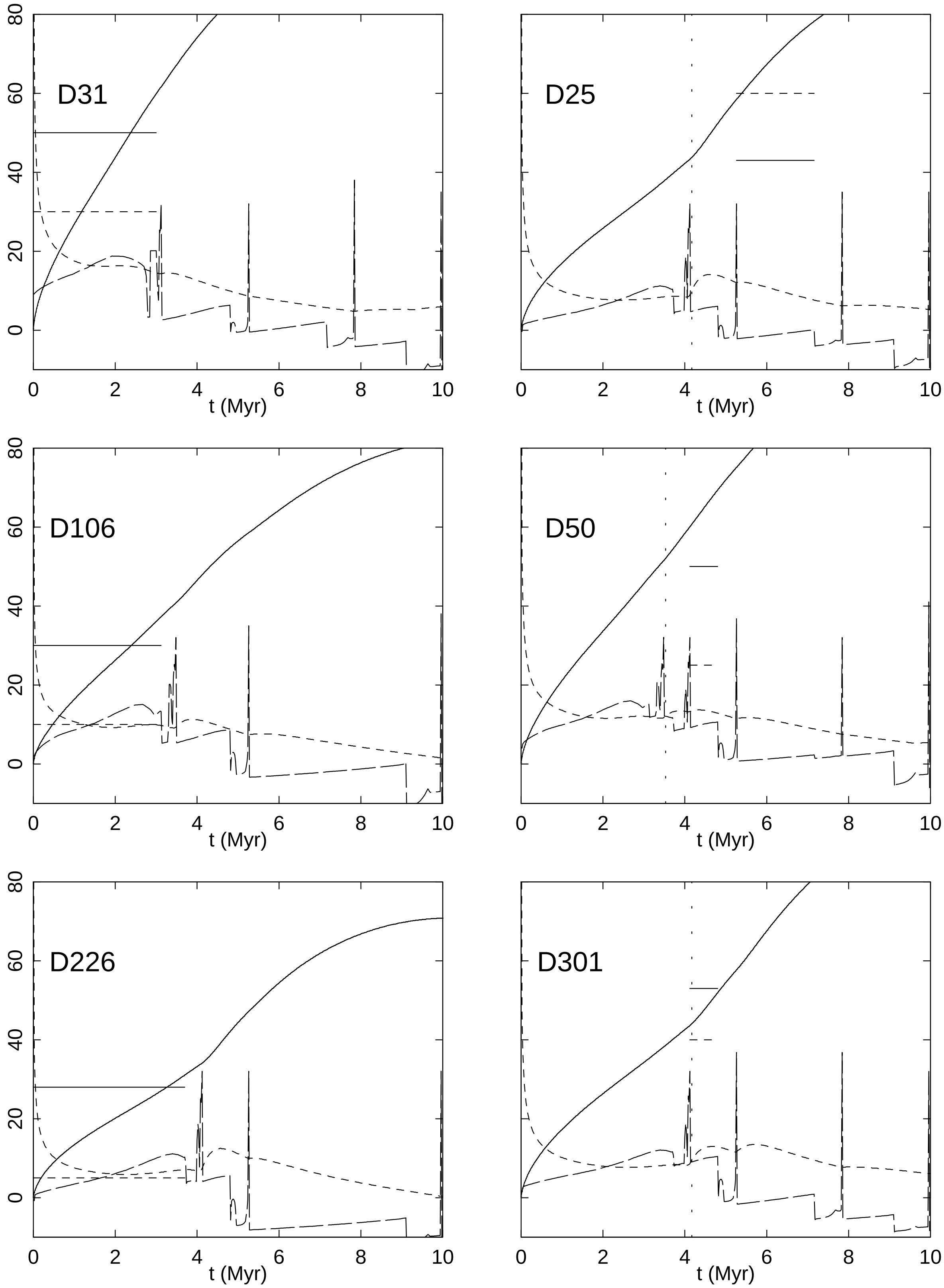

Fig. 4.— Left column shows the same models for low-velocity superbubbles as in Figure 2, but reducing L_w/n_0 by a factor of 10; right column shows same reduction of L_w/n_0 for high-velocity models shown in the right column of Figure 1.